https://doi.org/10.5194/os-2020-30
Preprint. Discussion started: 6 May 2020

Effects of current on wind waves in strong winds

Naohisa Takagaki[1], Naoya Suzuki[2], Yuliya Troitskaya[3], Chiaki Tanaka[2], Alexander Kandaurov[3], Maxim Vdovin[3]

[1] (Corresponding Author) Department of Mechanical Engineering, University of Hyogo, Shosha 2167, Himeji Hyogo, 671-2280 Japan, *E-mail: takagaki@eng.u-hyogo.ac.jp*
Tel/Fax: +81-79-267-47834

[2] Faculty of Science and Engineering, Kindai University, 3-4-1, Kowakae Higashiosaka Osaka, 577-8502 Japan.

[3] Department of Geophysical Research, Institute of Applied Physics, the Russian Academy of Sciences, 46 Ul'yanov Street, Nizhny Novgorod, 603-950, Russia.

Keywords: wind waves, current, Doppler shift

Abstract

It is important to investigate the effects of current on wind waves, called the Doppler shift, both at normal and extreme high wind speeds. Three different types of wind-wave tanks along with a fan and pump are used to demonstrate wind waves and currents in laboratories at Kyoto University, Japan, Kindai University, Japan, and the Institute of Applied Physics, Russian Academy of Sciences, Russia. Profiles of the wind and current velocities and the water-level fluctuation are measured. The wave frequency, wavelength, and phase velocity of the significant waves are calculated, and the water velocities at the water surface and in the bulk of the water are also estimated by the current distribution. The results show that 27 different types of currents can be generated at wind speeds ranging from 7 to 67 m s^{-1}. At normal wind speeds under 30 m s^{-1}, wave frequency, wavelength, and phase velocity depend on wind speed and fetch. The effect of the Doppler shift is confirmed at normal wind speeds, i.e., the significant waves are accelerated by the surface current. The phase velocity can be represented as the sum of the surface current and artificial phase velocity, which is estimated by the dispersion relation of the deep-water waves. At extreme high wind speeds, over 30 m s^{-1}, a similar Doppler shift is observed as under the conditions of normal wind speeds. This suggests that the Doppler shift is an adequate model for representing the acceleration of wind

https://doi.org/10.5194/os-2020-30
Preprint. Discussion started: 6 May 2020

waves by current, not only for the wind waves at normal wind speeds but also for those with intensive breaking at extreme high wind speeds. A weakly nonlinear model of surface waves at a shear flow is developed. It is shown that it describes well the dispersion properties of not only small-amplitude waves but also strongly nonlinear and even breaking waves, typical for extreme wind conditions (over 30 m s^{-1}).

1. Introduction

The oceans flow constantly, depending on the earth's rotation, tides, ground shape, and wind shear. High-speed continuous ocean flows are called currents. Although the mean surface velocity of the ocean is approximately 0.1 m s^{-1}, the maximum surface velocity for the currents is 1 m/s (e.g., Kawabe, 1988; Kelly et al., 2001). The interaction between the current and wind waves generated by the wind shear have been investigated in several studies. The acceleration effects of the current on wind waves (well known as the Doppler shift), the effects of the current on the momentum and heat transfer across a sea surface, and the modeling of waves and currents in the Gulf Stream have been the subject of experimental and numerical investigations (e.g., Dawe and Thompson, 2006; Kara et al., 2007; Fan et al., 2009; Shi and Bourassa, 2019). However, these studies were performed at normal wind speeds only, and few studies have been conducted at extreme high wind speeds, for which the threshold velocity is 30 – 35 m s^{-1}, representing the regime shift of the air-sea momentum, heat, and mass transport (Powell et al., 2003; Donelan et al., 2004; Takagaki et al., 2012, 2016; Troitskaya et al., 2012; Iwano et al., 2013; Krall and Jähne, 2014; Komori et al., 2018; Krall et al., 2019). At such extreme high wind speeds, owing to the intensive breaking by the strong wind shear, the local ocean flows might be strong. Furthermore, under a hurricane, the directions of the wind and ocean flows rapidly change; thus, the wind waves under a hurricane might be strongly affected by complicated local ocean flows. However, the effects of the current on wind waves have not yet been clarified.

Therefore, the purpose of this study is to investigate the effects of the current on wind waves in strong winds through the application of three different types of wind-wave tanks, along with a pump.

2. Experiment

2.1. Equipment and measurement methods

Wind-wave tanks at Kyoto University, Japan and the Institute of Applied Physics, Russian Academy of Sciences (IAP RAS) were used in the experiments (Figs. 1a, 1b). For the tank at Kyoto University, the glass test section was 15 m long, 0.8 m wide, and 1.6

https://doi.org/10.5194/os-2020-30
Preprint. Discussion started: 6 May 2020

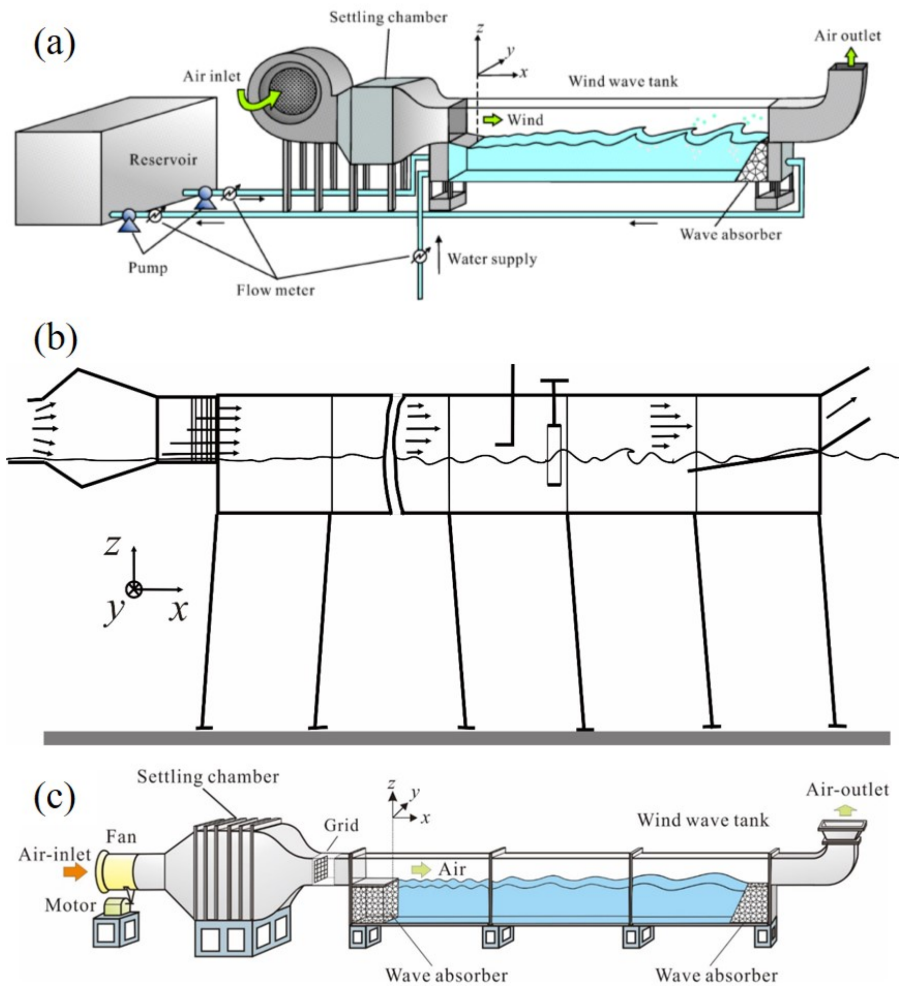

Figure 1. Schematics of wind-wave tanks. (a) High-speed wind-wave tank of Kyoto University. (b) Typhoon simulator of IAP RAS. (c) Wind-wave tank of Kindai University.

m high. The water depth *D* was set at 0.8 m. For the tank at IAP RAS, the test section in the air side was 15 m long, 0.4 m wide, and 0.4 m high. The water depth *D* was set at 1.5 m. The wind was set to blow over the filtered tap water in these tanks, generating wind waves. The wind speeds ranged from 4.7 to 43 m s^{-1} and from 8.5 to 21 m s^{-1} in the tanks at Kyoto and IAP RAS, respectively. Measurements of the wind speeds, water-level fluctuation, and current were carried out 6.5 m downstream from the edge (x = 0 m) in

https://doi.org/10.5194/os-2020-30
Preprint. Discussion started: 6 May 2020

both the Kyoto and IAP RAS tanks. Here, the *x*, *y*, and *z* coordinates are referred to as the streamwise, spanwise, and vertical directions, respectively, with the origin located at the center of the edge of the entrance plate. Additionally, the fetch (*x*) is defined as the distance between the origin and measurement point (x = 6.5 m).

In Kyoto, a laser Doppler anemometer (Dantec Dynamics LDA) and phase Doppler anemometer (Dantec Dynamics PDA) were used to measure the wind velocity fluctuation. A high-power multi-line argon-ion (Ar^+) laser (Lexel model 95-7; laser wavelengths of 488.0 and 514.5 nm) with a power of 3 W was used. The Ar^+ laser beam was shot through the sidewall (glass) of the tank. Scattered particles with a diameter of approximately 1 μm were produced by a fog generator (Dantec Dynamics F2010 Plus) and were fed into the air flow over the waves (see Takagaki et al. (2012) and Komori et al. (2018) for details). Water level fluctuations were measured using resistance-type wave gauges (Kenek CHT4-HR60BNC). The resistance wire was placed into the water, and the electrical resistance at the instantaneous water level was recorded at 500 Hz for 600 s using a digital recorder (Sony EX-UT10). The energy of the wind waves (E) was estimated by integrating the spectrum of the water-level fluctuations over the frequency (f). The values of the wavelength (L_S) and phase velocity (C_S) were estimated using the cospectra method (e.g., Takagaki et al., 2017). The current was measured using the same LDA system.

In IAP RAS, a hot-wire anemometer (E+E Electrinik EE75) was used to measure the representative mean wind velocity at x = 0.5 m and z = 0.2 m. The three wind velocities (U_{10}, $u*$, U_∞) at x = 6.5 m were taken from Troitskaya et al. (2012). The water-level fluctuations were measured using three handmade capacitive-type wave gauges. Three wires formed a triangle with 25 mm on a side. The wires were placed in the water, and the output voltages at the instantaneous water level were recorded at 200 Hz for 5400 s using a digital recorder through an AD converter (L-Card E14-140). The current was measured through acoustic Doppler velocimetry (Nortec AS) at x = 6.5 m and z = −10, −30, −50, −100, −150, −220, and −380 mm (see Troitskaya et al. (2012) for details).

2.2. Artificial current experiments at Kindai University

Additional experiments were performed using a wind-wave tank at Kindai University with a glass test section 6.5 m long, 0.3 m wide, and 0.8 m high (Fig. 1c). The water depth D was set at 0.49 m. A Pitot tube (Okano Works, LK-0) and differential manometers (Delta Ohm HD402T) were used to measure the mean wind velocity. The water level fluctuations were measured using resistance-type wave gauges (Kenek CHT4-HR60BNC). To measure L_S and C_P, another wave gauge was fixed downstream at

https://doi.org/10.5194/os-2020-30
Preprint. Discussion started: 6 May 2020

$\Delta x = 0.02$ m, where Δx is the interval between the two wave gauges. The current was then measured through electromagnetic velocimetry (Kenek LP3100) with a probe (Kenek LPT-200-09PS) at $x = 4.0$ m. The probe sensing station was 22 mm long with a diameter of 9 mm. The measurements were performed at $z = -15$ to -315 mm at 30 mm intervals. The sampling frequency was 8 Hz, and the sampling time was 180 s.

3. Results and discussion

3.1. Waves and current

Figure 2 shows the vertical distributions of the streamwise water velocity. The water velocities in the three different wind-wave tanks at Kyoto University, Kindai University, and IAP RAS are separately shown in each subfigure. In Fig. 2a, the bulk velocity of water U_{BULK} shows negative values ($U_{\mathrm{BULK}} = -0.16$ to -0.01 m s^{-1}) at Kyoto University, which is generated as the counterflow against the Stokes drift at the wavy water surface. In Fig. 2b, the bulk velocity of water demonstrates positive values (U_{BULK} = 0.019 to 0.044 m/s) at IAP RAS. This is because the wind-wave tank at IAP RAS is an open tank; thus, the Stokes drift on the wavy water surface does not provide the counterflow for the bulk water, unlike in the closed tank at Kyoto University. From Fig. 2c, it is clear that the bulk velocities of the water vary in each case at Kindai University with the use of the pump. Furthermore, the water bulk velocities change from negative to positive ($U_{\mathrm{BULK}} = -0.13$ to -0.17 m s^{-1}). The bulk velocities of water were defined as the mean velocity with $z = -0.4$ to -0.25 m (see dotted lines in Fig. 2), and the velocities are listed in Table 1. Experiments were performed under 27 different conditions, with the bulk velocity of water provided in the three different wind-wave tanks. The surface velocities of water, U_{SURF}, also varied in the three tanks with respect to wind speed (see Fig. 2). The U_{SURF} values were estimated by the linear extrapolation lines (dashed lines) as the water velocity at the surface ($z = 0$ m) shown in Fig. 2, and the velocities are listed in Table 1.

Figure 3 shows the wind-velocity dependency of the wave frequency f_{m}, wavelength L_{S}, phase velocity C_{S}, surface velocity of water U_{SURF}, and bulk velocity of water U_{BULK}. From Figs. 3a–3c, it is clear that both the Kyoto and IAP RAS data demonstrate that the wind waves develop with wind shear. Although f_{m} in both cases correspond to each other, L_{S} and C_{S} in IAP RAS are different from those in Kyoto. The disagreement might be caused by the difference in the wind-wave development or Doppler effect; this is discussed below. From Figs. 3d and 3e, U_{SURF} and U_{BULK} increase with an increase in U_{10} in IAP RAS. However, in Kyoto, U_{SURF} increases, but U_{BULK} decreases with an increase in U_{10}. Moreover, U_{SURF} in IAP RAS corresponds to U_{SURF} in

https://doi.org/10.5194/os-2020-30
Preprint. Discussion started: 6 May 2020

Ocean Science
Discussions
Open Access

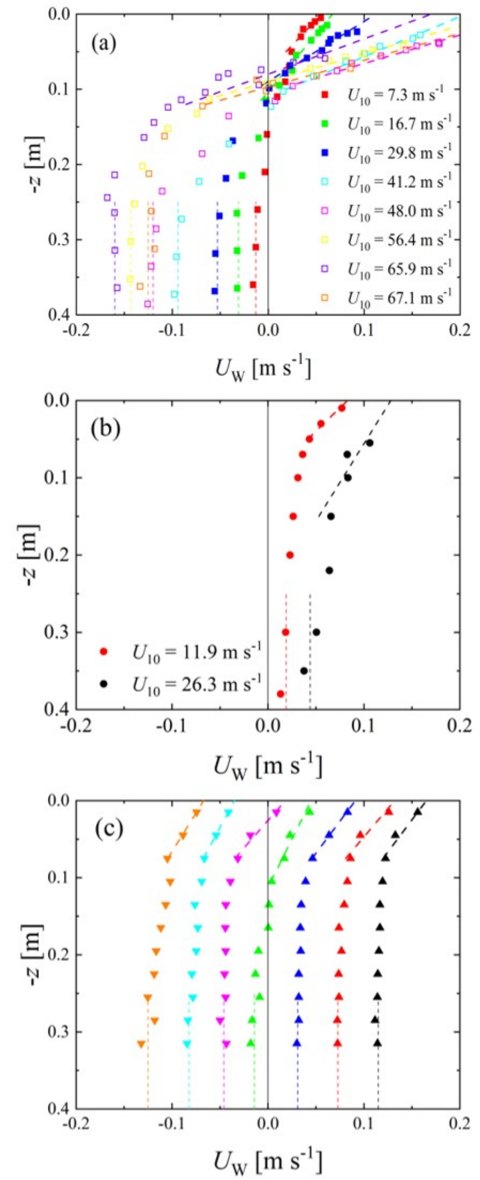

Figure 2. Vertical distributions of water-flow velocity; (a) Kyoto University, (b) IAP RAS, and (c) Kindai University. In (c), plots indicate cases 21–27 starting from right. Dotted and dashed lines indicate the lines used to estimate U_{BULK} and U_{SURF}, respectively. Open symbols show the high-wind-speed cases.

https://doi.org/10.5194/os-2020-30
Preprint. Discussion started: 6 May 2020

Ocean Science
Discussions
Open Access

TABLE 1. Wind and wind-wave properties. F: fetch; N_{PUMP}: pump inverter frequency; U_∞: freestream wind speed; u*: friction velocity of air; U_{10}: wind speed at 10 m above the sea surface; U_{SURF}: surface flow velocity of water; U_{BULK}: bulk flow velocity of water; C_D: drag coefficient; H_S: significant wave height; T_S: significant wave period; E: wave energy; f_m: significant frequency; C_S: phase velocity; L_S: significant wave length; $C_{S\text{-theor-l}}$: phase velocity predicted by theoretical linear model; $C_{S\text{-theor-nl}}$: phase velocity predicted by theoretical nonlinear model. The values of u*, U_{10}, and C_D in Kindai were estimated using the empirical curves by Iwano et al. (2013) from U_∞. Superscripts † and †† indicate the artificial following and opposing flows, respectively.

Case	Facility	F	N_{pump}	U_∞	u*	U_{10}	U_{SURF}	U_{BULK}	C_D	H_s	T_s	$E^{0.5}$	f_m	C_s	L_s	$C_{s\text{-theor-l}}$	$C_{s\text{-theor-nl}}$
		[m]	[Hz]	[m s^{-1}]	[m s^{-1}]	[m s^{-1}]	[m s^{-1}]	[m s^{-1}]	[×10^{-3}]	[m]	[m]	[m]	[Hz]	[m s^{-1}]	[m]	[m s^{-1}]	[m s^{-1}]
1	Kyoto	6.5	-	4.7	0.24	7.3	0.056	-0.01	1.1	0.0035	0.15	0.00092	6.63	0.40	0.06	0.369	0.374
2	Kyoto	6.5	-	7.2	0.43	11.5	-	-	1.4	0.0131	0.25	0.00353	3.95	0.59	0.16	-	-
3	Kyoto	6.5	-	10.3	0.67	16.7	0.067	-0.031	1.6	0.0231	0.32	0.00624	3.03	0.69	0.23	0.658	0.690
4	Kyoto	6.5	-	12.6	0.89	21.5	-	-	1.7	0.0357	0.39	0.00968	2.59	0.92	0.38	-	-
5	Kyoto	6.5	-	16.3	1.49	29.8	0.112	-0.053	2.5	0.0584	0.50	0.01570	2.01	1.09	0.52	0.972	1.044
6	Kyoto	6.5	-	18.8	1.70	33.6	-	-	2.5	0.0626	0.52	0.01691	1.89	1.18	0.60	-	-
7	Kyoto	6.5	-	22.2	2.08	41.2	0.206	-0.094	2.6	0.0631	0.53	0.01735	1.86	1.35	0.74	1.188	1.258
8	Kyoto	6.5	-	24.8	-	-	-	-	-	0.0668	0.55	0.01866	1.76	1.41	0.79	-	-
9	Kyoto	6.5	-	28.5	2.36	48.0	0.273	-0.120	2.4	0.0727	0.58	0.02058	1.68	1.54	0.93	1.325	1.424
10	Kyoto	6.5	-	31.1	-	-	-	-	-	0.0807	0.62	0.02309	1.58	1.60	1.07	-	-
11	Kyoto	6.5	-	34.8	2.69	56.4	0.241	-0.143	2.3	0.0944	0.68	0.02715	1.44	1.64	1.10	1.379	1.550
12	Kyoto	6.5	-	37.1	2.89	57.7	-	-	2.5	0.1043	0.73	0.03027	1.37	1.76	1.31	-	-
13	Kyoto	6.5	-	39.6	3.38	65.9	0.170	-0.160	2.6	0.1214	0.80	0.03553	1.20	1.84	1.51	1.531	1.694
14	Kyoto	6.5	-	43.3	3.31	67.1	0.272	-0.125	2.4	0.1609	0.93	0.04766	1.08	2.01	1.92	1.743	2.149
15	IAP RAS	6.5	-	8.5	0.40	11.9	0.083	0.019	1.1	0.0214	0.31	0.0056	3.14	0.78	0.25	0.690	0.715
16	IAP RAS	6.5	-	11.0	0.60	16.7	-	-	1.3	0.0305	0.36	0.0081	2.84	0.89	0.32	-	-
17	IAP RAS	6.5	-	13.5	0.90	21.9	-	-	1.7	0.0455	0.43	0.0121	2.41	1.07	0.45	-	-
18	IAP RAS	6.5	-	16.3	1.15	26.3	0.128	0.044	1.9	0.0790	0.50	0.0161	1.95	1.27	0.65	1.111	1.190
19	IAP RAS	6.5	-	18.9	1.50	32.5	-	-	2.1	0.0690	0.54	0.0246	1.85	1.37	0.74	-	-
20	IAP RAS	6.5	-	21.2	1.70	36.9	-	-	2.1	0.0847	0.60	0.0305	1.61	1.61	1.00	-	-
21	Kindai	4.0	15†	5.8	0.28	7.9	0.165	0.115	1.2	0.0044	0.14	0.0012	6.92	0.43	0.06	0.484	0.492
22	Kindai	4.0	10†	5.8	0.28	7.9	0.132	0.073	1.2	0.0050	0.16	0.0014	6.10	0.43	0.07	0.501	0.510
23	Kindai	4.0	5†	5.8	0.28	7.9	0.091	0.031	1.2	0.0049	0.16	0.0014	6.16	0.38	0.06	0.410	0.420
24	Kindai	4.0	0	5.8	0.28	7.9	0.045	-0.014	1.2	0.0054	0.19	0.0014	5.47	0.38	0.07	0.382	0.393
25	Kindai	4.0	5††	5.8	0.28	7.9	0.018	-0.046	1.2	0.0076	0.23	0.0021	4.25	0.36	0.08	0.384	0.400
26	Kindai	4.0	10††	5.8	0.28	7.9	-0.035	-0.082	1.2	0.0098	0.27	0.0027	3.64	0.35	0.10	0.355	0.375
27	Kindai	4.0	15††	5.8	0.28	7.9	-0.067	-0.125	1.2	0.0125	0.34	0.0035	2.94	0.38	0.13	0.381	0.402

Kyoto. This is because the Stokes drift generated by the wind waves, rather than the current, is significant. For the Kindai data, although f_m, U_{SURF}, and U_{BULK} vary, L_S and C_S are concentrated at single points at L_S = 0.1 m and C_S = 0.4 m s^{-1}, respectively. This shows that the intensity and direction of the current do not significantly affect L_S and C_S but do affect f_m and U_{SURF}. Thus, this implies that the present artificial current changes the water flow dramatically but does not affect the development of the wind waves.

https://doi.org/10.5194/os-2020-30
Preprint. Discussion started: 6 May 2020

Ocean Science
Discussions

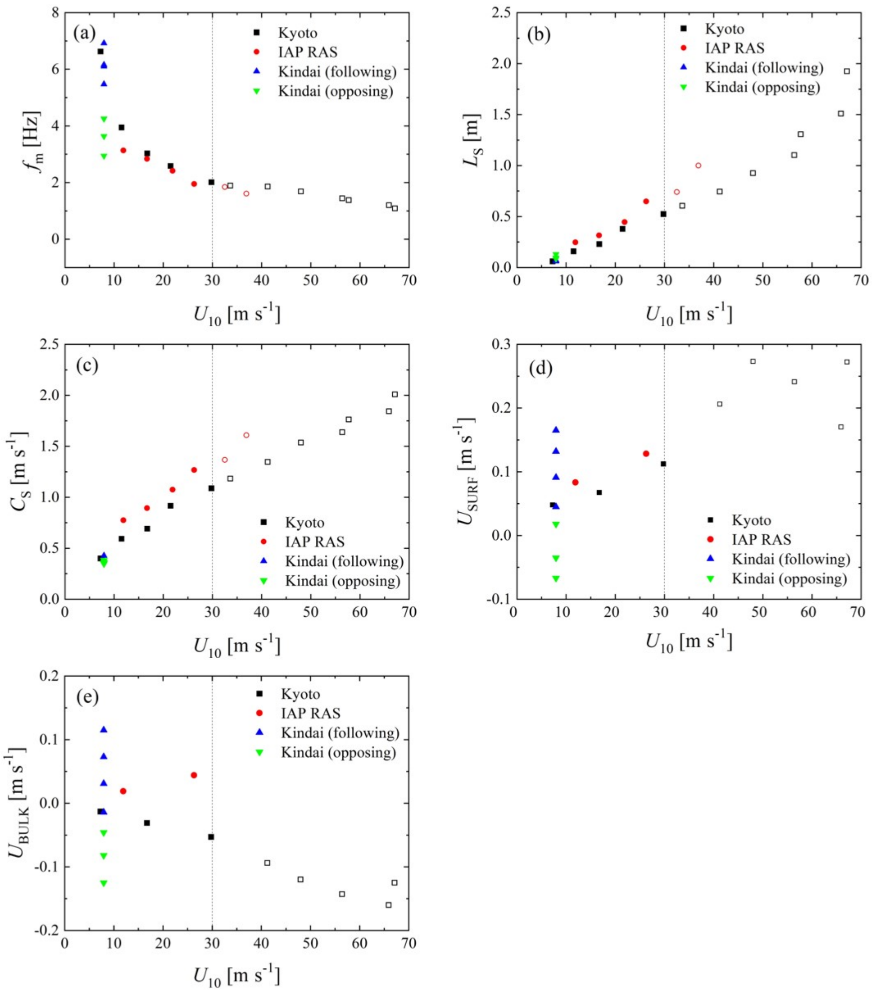

Figure 3. Relationships between U_{10} and (a) significant frequency f_m, (b) significant wave length L_S, (c) phase velocity C_S, (d) surface velocity of water U_{SURF}, and (e) bulk velocity of water U_{BULK}. Open symbols show the high-wind-speed cases.

Figure 4 shows the dispersion relation and demonstrates that the Kindai data points depend on the variation in the water velocity of the artificial current. The plots for the Kyoto University and IAP RAS cases at normal wind speeds (solid symbols) are

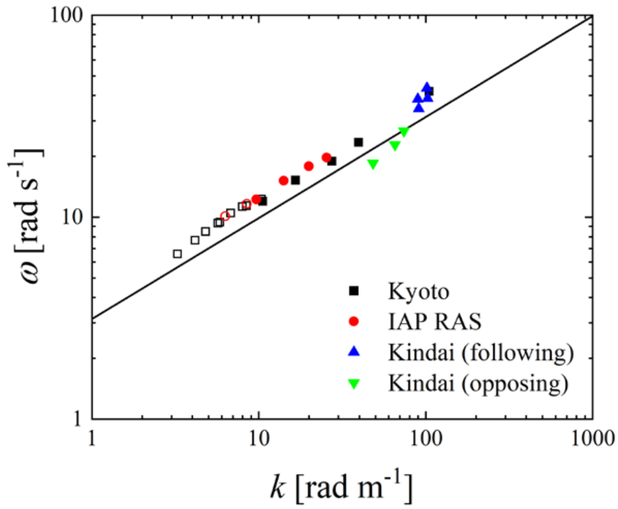

Figure 4. Dispersion relation between angular frequency ω and wave number k. Open symbols show the high-wind-speed cases. Curve shows the dispersion relation of the deep-water waves ($\omega^2 = gk$).

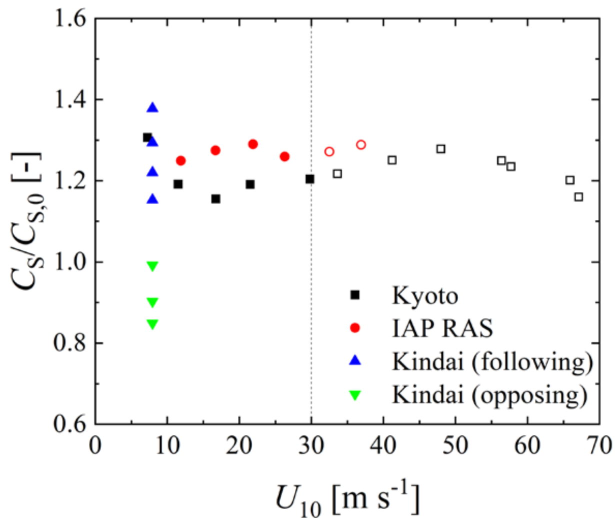

Figure 5. Relationship between the freestream wind speed and phase velocity C_S. The C_S is normalized by phase velocity $C_{S,0}$ without the Doppler effect, estimated by the dispersion relation of the deep-water waves ($C_{S,0} = (gL_S/2\pi)^{1/2}$). Open symbols show the high-wind-speed cases.

https://doi.org/10.5194/os-2020-30
Preprint. Discussion started: 6 May 2020

Ocean Science Discussions

concentrated above the solid curve, showing the dispersion relation of the deep-water waves ($\omega^2 = gk$). Meanwhile, the plots for extreme high wind speeds (open symbols) are also concentrated above the solid curve. This implies that the wind waves, along with the intensive breaking at extreme high wind speeds, are dependent on the Doppler shift. To investigate the phase velocity trend, Fig. 5 shows the ratio of the measured phase velocity C_S to the phase velocity $C_{S,0}$ estimated by the dispersion relation of the deep-water waves ($C_{S,0} = (gL_S/2\pi)^{1/2}$) against the wind velocity. From the figure, the ratios at the normal wind speeds assume a constant value (~1.21 in Kyoto or ~1.27 in IAP RAS). Moreover, the ratios at the extreme high wind speeds take similar values of 1.23 and 1.28 for Kyoto or IAP RAS, respectively. This implies that the phase velocities at extreme high wind speeds are accelerated by the current just as those at normal wind speeds. However, the Kindai values are scattered and increase in the following cases and decrease in the opposing cases. It is clear that the artificial current accelerates (or decelerates) the phase velocity.

To interpret the relationship among the measured phase velocity C_S, first phase velocity $C_{S,0}$ estimated by the dispersion relation, and water velocity, two types of phase velocity were evaluated: the sum of $C_{S,0}$ and surface velocity of water U_{SURF} and the sum of $C_{S,0}$ and bulk velocity of water U_{BULK}. Figure 6 shows the relationship between C_S and (a) $C_{S,0} + U_{SURF}$, and (b) $C_{S,0} + U_{BULK}$. In Fig. 6a, we can see that the Doppler shift is confirmed at the normal wind speeds, i.e., the significant waves are accelerated by the surface flow, and the real phase velocity can be represented as the sum of the velocity of the surface flow and the virtual phase velocity, which is estimated by the dispersion relation of the deep-water waves. At extreme high wind speeds over 30 m s^{-1}, a similar Doppler shift is observed as under the conditions of normal wind speeds, as seen in Fig. 6a. Meanwhile, in Fig. 6b, although C_S corresponds to $C_{S,0} + U_{BULK}$ at low phase velocities, C_S assumes values larger than $C_{S,0} + U_{BULK}$ at high phase velocities. This suggests that the Doppler shift is an adequate model for representing the acceleration of the wind waves by the current, not only for the wind waves at normal wind speeds but also for those with intensive breaking at extreme high wind speeds. Moreover, the Doppler shift of wind waves occurs due to a very thin surface flow, as the correlation between C_S and $C_{S,0} + U_{SURF}$ is higher than the correlation between C_S and $C_{S,0} + U_{BULK}$.

https://doi.org/10.5194/os-2020-30
Preprint. Discussion started: 6 May 2020

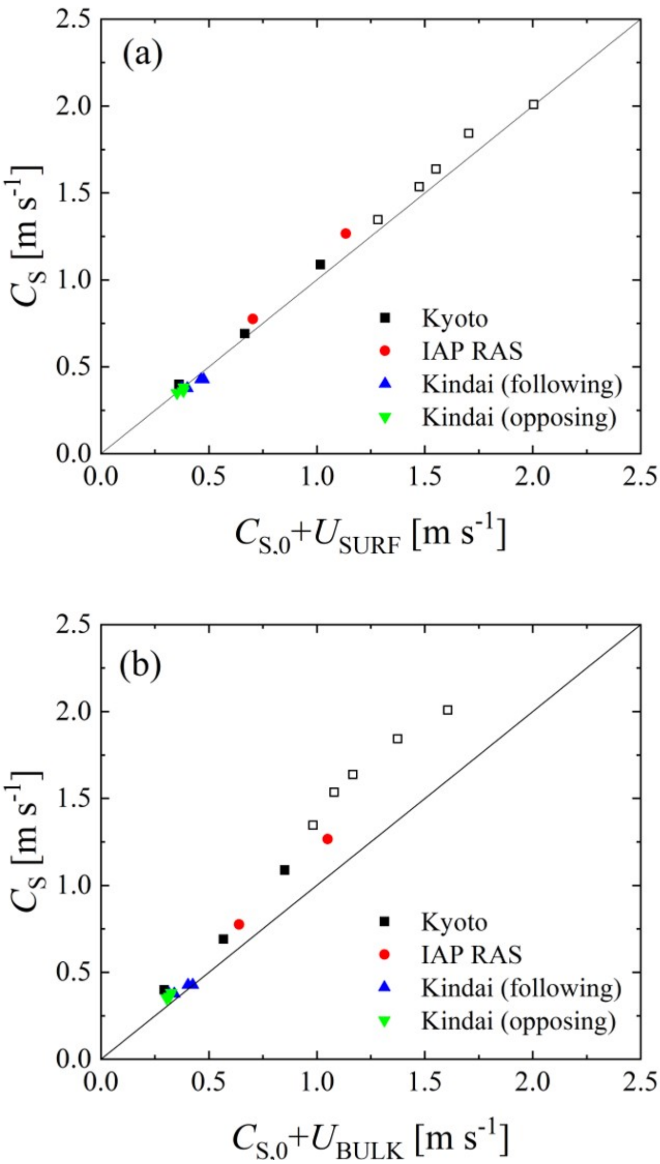

Figure 6. Relationship between phase velocity C_S and (a) sum of $C_{S,0}$ and surface velocity of water U_{SURF}, and (b) sum of $C_{S,0}$ and bulk velocity of water U_{BULK}. Open symbols show the high-wind-speed cases.

3.2. The theoretical model of waves at the shear flow

The parameters of the observed Doppler shift can be explained more precisely within the theoretical model of the capillary-gravity waves at the surface of the water flows with the velocity profiles prescribed by the experimental data, which are plotted in Fig. 2a–c. Because the dominant wind wave propagates along the wave and water flows, we will consider the 2D-wave model in the 2D flow. This flow is described by the system of 2D Euler equations:

$$\frac{\partial u}{\partial t}+u\frac{\partial u}{\partial x}+w\frac{\partial u}{\partial z}+\frac{1}{\rho}\frac{\partial p}{\partial x}=0, \quad (1)$$

$$\frac{\partial w}{\partial t}+u\frac{\partial w}{\partial x}+w\frac{\partial w}{\partial z}+\frac{1}{\rho}\frac{\partial p}{\partial z}=-g,$$

and the condition of non-compressibility:

$$\frac{\partial u}{\partial x}+\frac{\partial w}{\partial z}=0, \quad (2)$$

with the kinematical

$$\frac{\partial \eta}{\partial t}+u\frac{\partial \eta}{\partial x}=w\big|_{z=\eta(x,t)} \quad (3)$$

and dynamical boundary conditions

$$p\big|_{z=\eta(x,t)}=0 \quad (4)$$

at the water surface. Here, u and w are the horizontal and vertical velocity components, p is the water pressure, x and z are the horizontal and upward vertical coordinates, g is the gravity acceleration, and ρ is the water density. The boundary condition at the bottom of the channel is $w\big|_{z=-D}=0$. It should be noted that the water depth in almost all the experimental runs exceeded half of the wavelength of the dominant waves (see Table 1). In this case, the deep-water approximation is applicable for describing the surface waves, and the boundary condition of the wave field vanishing with the distance from the water surface can also be used.

Because the fluid motion under consideration is 2D, the stream function can be introduced as follows:

$$u=\frac{\partial \psi}{\partial z};w=-\frac{\partial \psi}{\partial x}. \quad (5)$$

To derive the linear dispersion relation for the surface waves at the plane shear flow with the horizontal velocity profile $U_w(z)$, we consider the solution to Eqs. (1, 2) in terms of the stream function as the sum of the undisturbed state with steady shear flow and

https://doi.org/10.5194/os-2020-30
Preprint. Discussion started: 6 May 2020

Ocean Science
Discussions
Open Access
EGU

small-amplitude disturbances. Then, the stream function ψ and pressure p are as follows:

$$\psi(x,z,t) = \int^{z} U_w(z_1)\,dz_1 + \varepsilon\psi_1(x,z,t); \tag{6}$$

$$p(x,z,t) = -\rho g z + \varepsilon p_1(x,z,t), \tag{7}$$

where $\varepsilon << 1$, and the water elevation value is also the order of ε, namely $\varepsilon\eta_1(x, t)$.

In the linear approximation in ε, the system of Eqs. (1, 2) and the boundary conditions of Eqs. (3, 4) take the form:

$$\begin{gathered}\left(\frac{\partial}{\partial t} + \frac{U_w(z)\partial}{\partial x}\right)\left(\frac{\partial^2\psi_1}{\partial x^2} + \frac{\partial^2\psi_1}{\partial z^2}\right) - \frac{\partial\psi_1}{\partial x}\frac{d^2U_w(z)}{dz^2} = 0,\\ \frac{\partial\eta_1}{\partial t} + U_w(0)\frac{\partial\eta_1}{\partial x} = -\left.\frac{\partial\psi_1}{\partial x}\right|_{z=0},\\ \left.\frac{\partial p_1}{\partial x}\right|_{z=0} - \rho g\frac{\partial\eta_1}{\partial x} = 0,\\ \left.\psi_1\right|_{z=-D} = 0.\end{gathered} \tag{8}$$

Excluding p_1 with use of the first equation of the system in Eq. (1) and eliminating η_1 yields one boundary condition at the water surface for ψ_1:

$$\left.\left[\left(\frac{\partial}{\partial t} + \frac{U_w(0)\partial}{\partial x}\right)^2\frac{\partial\psi_1}{\partial z} - \left(\frac{\partial}{\partial t} + U_w(0)\frac{\partial}{\partial x}\right)\frac{\partial\psi_1}{\partial x}\frac{dU_w}{dz} - g\frac{\partial^2\psi_1}{\partial x^2}\right]\right|_{z=0} = 0. \tag{9}$$

For the harmonic wave disturbance, where

$$\psi_1(x,z,t) = \Psi(t)\exp(-i(\omega t - kt)), \tag{10}$$

substituting into Eqs. (8, 9) yields the Rayleigh equation for the complex amplitude of the stream function disturbance:

$$(\omega - U_w(z)k)\left(\frac{d^2\Psi_1}{dz^2} - k^2\Psi_1\right) + \frac{d^2U_w(z)}{dz^2}k^2\Psi_1 = 0, \tag{11}$$

with the following boundary condition:

$$\begin{gathered}(\omega - U_w(0)k)^2\frac{d\Psi_1(0)}{dz} + (\omega - U_w(0)k)k\Psi_1(0)\frac{dU_w(0)}{dz} - k^2 g\Psi_1(0) = 0,\\ \left.\Psi_1\right|_{z\to-\infty} \to 0.\end{gathered} \tag{12}$$

Numerically solving the boundary layer problem for Eq. (11) with the boundary conditions in Eq. (12) enables one to obtain the dispersion relation $\omega(k)$ for the surface waves at the inhomogeneous shear flow. Note that because the phase velocity of the waves significantly exceeded the flow velocity in all experiments (cf. Figs. 2 and 3), the Rayleigh equation did not have a singularity, and the calculated frequency and phase

https://doi.org/10.5194/os-2020-30
Preprint. Discussion started: 6 May 2020

Ocean Science Discussions
Open Access
EGU

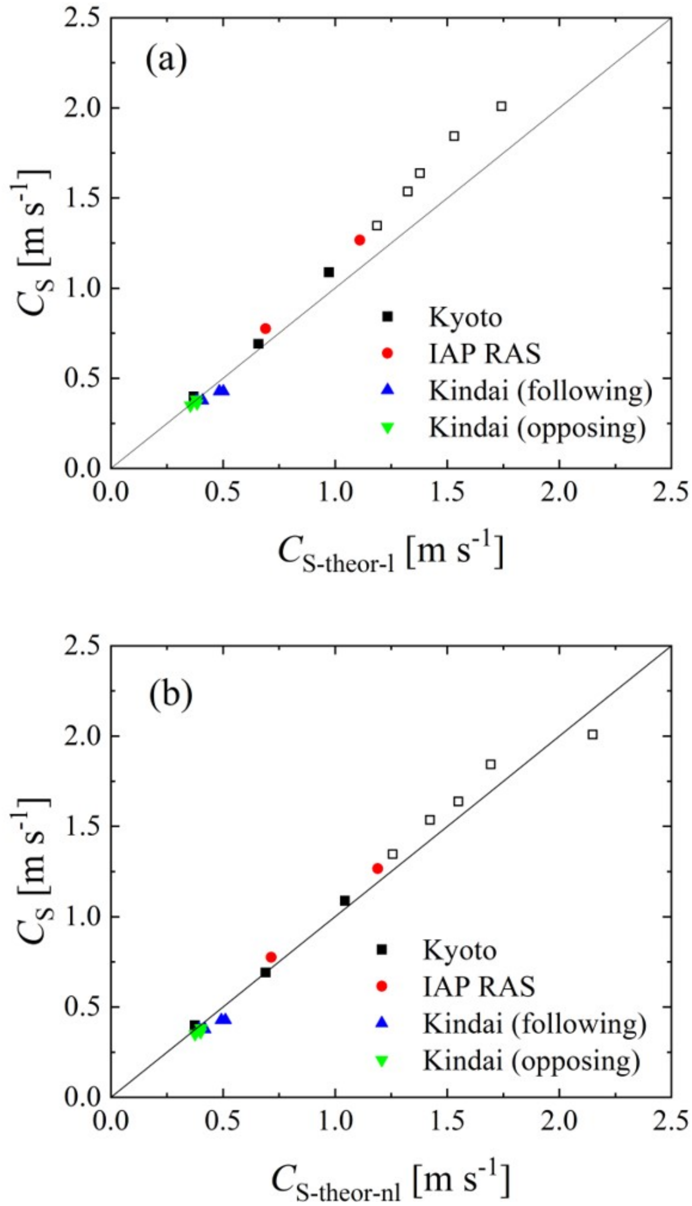

Figure 7. The measured phase velocity C_S versus theoretical prediction: (a) linear model, and (b) nonlinear model.

https://doi.org/10.5194/os-2020-30
Preprint. Discussion started: 6 May 2020

Ocean Science
Discussions
Open Access

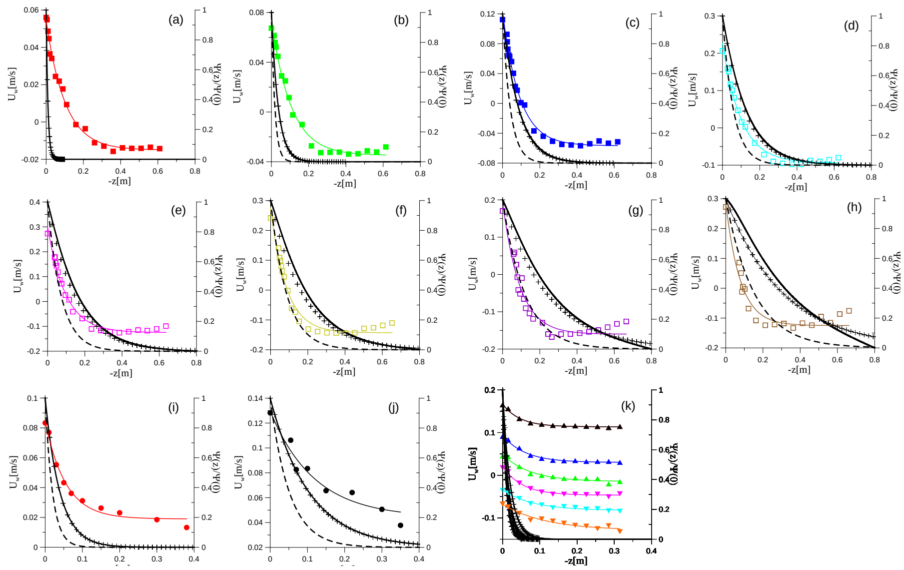

Figure 8. Vertical velocity profiles (points), their fitting (thin color line), the eigenfunction of the Eq. (8) with the boundary conditions Eq. (9) (black solid curve), the function e^{kz} (crosses), the function e^{2kz} (dashed line). The panels (a)-(j) corresponds to the experiments No. 1, 3, 5, 7, 9, 11, 13-15, 18 respectively, the panel (k) corresponds to the experiments No. 21-27.

velocity of the wave were real values, i.e., the current was neutral stable.

The wave phase velocities $C_{\text{S-theor-l}} = \omega(k)/k$ were calculated for the parameters of those experiments that contained complete information about the course and characteristics of the waves, namely 1, 3, 5, 7, 9, 11, 13–15, 18, and 21–27 from Table 1. The results are presented in Fig. 7a as the measured phase velocity Cs versus calculated phase velocity $C_{\text{S-theor-l}}$. One can see that the model corresponds to the data substantially better than does the model of linear potential waves at the homogeneous current U_{BULK} (compare Fig. 6b). Considering the structure of the wave disturbances of the stream function, $\Psi_1(z)$, which was found as the eigenfunction of the boundary problem of Eqs. (11, 12). The profiles of $\Psi_1(z)$ are presented in Fig. 8. One can see that in all cases the functions $\Psi_1(z)$ are close to e^{kz} at the background of the mean velocity profiles. Moreover, for experiments No. 1, 3, 5, 15, and 21–27 (see Fig. 8a, 8b, 8c, 8i, and 8k), the wave field is concentrated near the surface at a distance less than the scale of the change in the mean flow, where the flow velocity is approximately equal to U_{SURF}. This explains the good correlation in these cases of the observed phase velocity with the phase velocity of waves

https://doi.org/10.5194/os-2020-30
Preprint. Discussion started: 6 May 2020

Ocean Science Discussions

at the homogeneous current U_{SURF} presented in Fig. 6a. At the same time, for experiments No. 7, 9, 5, 11, 13, 14, and 18 (see Figs. 8d–8h, and 8j), the scale of the variability of the flow is significantly smaller than the scale of the wave field. Under these conditions, a significant difference between the phase velocity of the waves and that given by the linear dispersion relation can be due to the influence of nonlinearity.

To estimate the nonlinear addition to the wave phase velocity, we used the results of the weakly nonlinear theory of surface waves for the current with a constant shear. Of course, the flow in the experiments of the present work does not have a constant shift, and this was considered when obtaining the linear dispersion relation. However, it should be taken into account that the contributions of the *n*-th harmonic to the nonlinear dispersion relation are determined by wave fields in the *n*-power, which have a scale that is *n* time smaller than the first harmonic. Additionally, the model of constant shear of the mean current velocity is already approximately applicable for the 2nd harmonic (see Fig. 8).

We use the nonlinear dispersion relation for waves in the current with a constant shift in the deep-water approximation, which was obtained by Simmen and Saffman (1985):

$$(\omega - U_w(0)k)^2 \frac{d\Psi_1(0)}{dz} + (\omega - U_w(0)k)k\Psi_1(0)\frac{dU_w(0)}{dz} - k^2 g\Psi_1(0) = \gamma(ka)^2,$$

$$\gamma = \frac{(\omega_0 - U_w(0)k)^2}{2k}\left(1-\frac{1}{2}\Omega^2 + \left(1+2\Omega+\frac{1}{2}\Omega^2\right)^2\right), \qquad (13)$$

$$\Omega = \frac{1}{(\omega_0 - U_w(0)k)}\frac{dU_w(0)}{dz},$$

Here, ω_0 is the solution of the linear dispersion equation. Eq. (13) is rewritten in the notation of this work and formulated in a reference frame in which the surface of the water has the velocity $U_w(0)$. Note that the linear part of Eq. (13) coincides with Eq. (12). The results of solving Eq. (13) are presented in Fig. 7b similarly to Fig. 7a as the measured phase velocity C_S versus calculated phase velocity $C_{S\text{-theor-nl}} = \omega(k)/k$, where one can see their good agreement with each other. Thus, the wave frequency shift can be explained by two factors, including the Doppler shift at the mean flow and the nonlinear frequency shift, while, the latter can also be interpreted in its physical nature as the wave frequency shift in the presence of its orbital velocities.

Recent studies have indicated a regime shift in the momentum, heat, and mass transfer across an intensive broken wave surface along with the amount of dispersed droplets and entrained bubbles at extreme high wind speeds over 30 m s^{-1} (e.g., Powell et al., 2003; Donelan et al., 2004; Takagaki et al., 2012, 2016; Troitskaya et al., 2012; Iwano et al., 2013; Krall and Jähne, 2014; Komori et al., 2018; Krall et al., 2019). Thus, there is

https://doi.org/10.5194/os-2020-30
Preprint. Discussion started: 6 May 2020

the possibility of a similar regime shift in the Doppler shift of wind waves by the current at extreme high wind speeds. However, the present study reveals that such a Doppler shift is observed as under the conditions of normal wind speeds. In this case, the weakly nonlinear approximation turns out to be applicable for describing the dispersion properties of not only small-amplitude waves but also nonlinear and even breaking waves. This implies that the intensive wave breaking at extreme high wind speeds occurs with the saturation (or dumping) of the wave height rather than the wavelength. This evidence might be helpful in investigating and modelling the wind-wave development at extreme high wind speeds.

4. Conclusion

The effects of the current on wind waves were investigated through laboratory experiments in three different wind-wave tanks along with a pump at Kyoto University, Japan, Kindai University, Japan, and IAP RAS. In this experiment, 27 different types of currents were generated at wind speeds ranging from 7 to 67 m s^{-1}. At normal wind speeds under 30 m s^{-1}, the wave frequency, wavelength, phase velocity of waves, and surface velocity of the water were found to depend on the wind speed. However, the bulk velocity of the water showed a dependence on the tank type, i.e., open tank (IAP RAS) or closed tank (Kyoto University). The effect of the Doppler shift was confirmed at normal wind speeds, i.e., the significant waves were accelerated by the surface flow, and the phase velocity was represented as the sum of the surface velocity of water and the phase velocity, which is estimated by the dispersion relation of the deep-water waves. At extreme high wind speeds over 30 m s^{-1}, a Doppler shift was observed similar to that under the conditions of normal wind speeds. This suggests that the Doppler shift is an adequate model for representing the acceleration of wind waves by the current, not only for the wind waves at normal wind speeds but also for those with intensive breaking at extreme high wind speeds. The data obtained by the artificial current experiments conducted at Kindai University were used to explain how the artificial current accelerates (or decelerates) the significant waves. A weakly nonlinear model of surface waves at a shear flow was developed. It was shown that it describes well the dispersion properties of not only small-amplitude waves but also strongly nonlinear and even breaking waves, typical for extreme wind conditions, with speeds, U_{10}, exceeding 30 m s^{-1}.

Acknowledgements

This work was supported by the Ministry of Education, Culture, Sports, Science and Technology (Grant-in-Aid No's. 18H01284, 18K03953, and 19KK0087). This project was supported by the Japan Society for the Promotion of Science and the Russian Foundation for Basic Research under the Japan-Russia Research Cooperative Program. We thank Prof. S. Komori and Mr. Tsuji for their help in conducting the experiments and for useful discussions. The experiments of IAP RAS were performed at the Unique Scientific Facility "Complex of Large-Scale Geophysical Facilities" (http://www.ckp-rf.ru/usu/77738/).

References

Dawe, J. T., Thompson, L., (2006), Effect of ocean surface currents on wind stress, heat flux, and wind power input to the ocean, Geophysical Research Letters, 33, L09604, doi:10.1029/2006GL025784

Donelan, M.A., Haus, B.K., Reul, N., Plant, W.J., Stiassnie, M., Graber, H.C., Brown, O.B., Saltzman, E.S., (2004), On the limiting aerodynamic roughness of the ocean in very strong winds, Geophysical Research Letters, 31, doi:10.1029/2004GL019460. L18306

Fan, Y., Ginis, I., Hara, T., (2009), The Effect of Wind–Wave–Current Interaction on Air–Sea Momentum Fluxes and Ocean Response in Tropical Cyclones, Journal of Physical Oceanography, 39, pp. 1019-1034.

Iwano, K., Takagaki, N., Kurose, R., Komori, S., (2013), Mass transfer velocity across the breaking air-water interface at extremely high wind speeds, Tellus B 65, 21341, doi:10.3402/tellusb.v65i0.21341

Kara, A. B., Metzger, E. J., Bourassa, M. A., (2007), Ocean current and wave effects on wind stress drag coefficient over the global ocean, Geophysical Research Letters, 34, L01604, doi:10.1029/2006GL027849

Kawabe, M., (1988), Variability of Kuroshio velocity assessed from the sea-level difference between Naze and Nishinoomote, Journal of oceanographical Society of Japan, 44, pp. 293-304.

Kelly, K. A., Dickinson, S., McPhaden, M. J., Johnson, G. C., (2001), Ocean currents evident in satellite wind data, Geophysical Research Letters, 28(12), pp. 2469-2472.

Komori, S., Iwano, K., Takagaki, N., Onishi, R., Kurose, R., Takahashi, K., Suzuki, N., (2018), Laboratory measurements of heat transfer and drag coefficients at

https://doi.org/10.5194/os-2020-30
Preprint. Discussion started: 6 May 2020

Ocean Science Discussions
Open Access

extremely high wind speeds, Journal of Physical Oceanography, doi:10.1175/JPO-D-17-0243.1

Krall, K. E., Jähne, B., (2014), First laboratory study of air-sea gas exchange at hurricane wind speeds, Ocean Science, 10(2), 257-265, doi:10.5194/os-10-257-2014

Krall, K. E., Smith, A. W., Takagaki, N., Jähne, B., (2019), Air–sea gas exchange at wind speeds up to 85 m s-1, Ocean Science, 15(6), doi: 10.5194/os-15-1783-2019

Powell, M. D., Vickery, P. J., Reinhold, T. A., (2003), Reduced drag coefficient for high wind speeds in tropical cyclones, Nature, 422, 279–283, doi:10.1038/nature01481

Shi, Q., Bourassa, M. A., (2019), Coupling Ocean Currents and Waves with Wind Stress over the Gulf Stream, Remote Sensing, 11, 1476, doi:10.3390/rs11121476

Simmen, J. A., Saffman, P. G., (1985), Steady deep-water waves on a linear shear current, Studies in Applied Mathematics, 73, 35–57, doi: 10.1002/sapm198573135

Takagaki, N., Komori, S., Suzuki, N., Iwano, K., Kuramoto, T., Shimada, S., Kurose, R., Takahashi, K., (2012), Strong correlation between the drag coefficient and the shape of the wind sea spectrum over a broad range of wind speeds, Geophysical Research Letters, 39, doi:10.1029/2012GL053988. L23604

Takagaki, N., Komori, S., Suzuki, N., Iwano, K., Kurose, R., (2016), Mechanism of drag coefficient saturation at strong wind speeds, Geophysical Research Letters, 43, doi:10.1002/2016GL070666

Takagaki, N., Komori, S., Ishida, M., Iwano, K., Kurose, R., Suzuki, N., (2017), Loop-type wave-generation method for generating wind waves under long-fetch conditions, Journal of Atmospheric Oceanic Technology, 34(10), 2129–2139, doi:10.1175/JTECH-D-17-0043.1

Troitskaya, Y. I., Sergeev, D. A., Kandaurov, A. A., Baidakov, G. A., Vdovin, M. A., Kazakov, V. I., (2012), Laboratory and theoretical modeling of air-sea momentum transfer under severe wind conditions, Journal of Geophysical Research, 117, C00J21, doi:10.1029/2011JC007778